Joint Beamforming Design in Reconfigurable Intelligent Surface-Assisted Rate Splitting Networks

Ticao Zhang and Shiwen Mao, *Fellow, IEEE*

***Abstract*—Reconfigurable Intelligent Surface (RIS) is an emerging technology that can improve the spectrum and energy efficiency of next-generation wireless networks. However, attaining accurate channel state information (CSI) for the cascaded RIS channel is particularly challenging. Imperfect CSI is a major bottleneck to achieving the spectral efficiency benefit of RIS-assisted networks. Rate splitting (RS), a promising multiple access technology, has been shown to be able to achieve an improved spectrum efficiency and be robust to channel uncertainties. This paper investigates the interplay between RIS and RS by considering a RIS-assisted RS beamforming problem. Active beamforming at the base station (BS) and passive beamforming at the RIS are jointly considered to maximize the minimum user rate under both the perfect CSI case and the imperfect CSI case. A block coordinate descent (BCD) algorithm is developed to solve this non-convex problem. Compared with the conventional semi-definite relaxation (SDR) approach, the proposed method does not require that the covariance matrix of the common beamforming vector be rank-one. Moreover, we present theoretical results to help reveal the impact of the system parameters and explain the performance gain resulting from the integration of RIS and RS. Extensive simulation results are also provided to show that RIS-assisted RS can improve the max-min rate performance significantly compared with conventional multiple access technologies, such as non-orthogonal multiple access (NOMA) and space division multiple access (SDMA) with/without RIS, especially in overloaded systems. With the proposed method, RS shows great potential in combating realistic CSI errors in RIS-assisted networks.**

***Index Terms*—Max-min fairness, rate splitting, reconfigurable intelligent surface (RIS), block coordinate descent (BCD).**

I. Introduction

Reconfigurable Intelligent Surface (RIS) has recently emerged as a promising technology for 6G wireless communications due to its ability to reconfigure the propagation environment [1]–[3]. RIS is a programmable meta-surface equipped with multiple low-cost programmable reflecting elements, whose amplitude and phase can be reconfigured. As a result, the reflection of incoming signals can be programmed to enhance the wireless channel. Compared with conventional technologies such as amplify-and-forward (AF), massive multiple-input multiple-output (MIMO) [4], and millimeter wave (mmWave), RIS does not require an increased number of active radio frequency (RF) chains. Both the energy consumption and hardware cost are low. RIS has been regarded as a promising technology for 6G to make high spectrum efficient, yet cost-effective systems.

Meanwhile, rate splitting (RS) has been envisioned as a promising multiple access technology for beyond 5G wireless communication [5]–[7]. In RS, the message at the transmitter is split into the private part and the common part. The common part shared a common codebook known to all users, hence can be decoded by each user. The private part can be decoded by removing the interference from the common part and treating interfering signals from other users as noise. The flexibility to partially decode interference and partially treat the remaining interference as noise makes RS a promising PHY-layer transmission paradigm for non-orthogonal transmission, interference management, and multiple access strategies in 6G [8]. RS has been shown in [9] to outperform and unify space division multiple access (SDMA) and non-orthogonal multiple access (NOMA) under a wide range of network loads and user deployment. Recent research progress has shown that RS can achieve a spectrum efficiency improvement [9], robust to imperfect channel state information (CSI) conditions [5], [10], and outperforms NOMA and SDMA in secure downlink transmissions [11].

Inspired by the appealing advantages of RIS and RS, researchers have begun to study the interplay and benefit of integrating the two infrastructure-level techniques. The benefits of integrating RIS and RS have been shown in terms of energy efficiency improvement [12], [13], secure transmission [14], spectrum efficiency improvement [15] and outage probabilities performance improvement [16]. Apart from these benefits, [17] tries to answer the question "Why we should consider the integration of RS and RIS" by showing that RS and RIS share similarities and they complement each other. To be specific, both techniques perform beamforming. RIS plays passive beamforming to assist the signal transmission while the RS plays active beamforming at the BS to achieve better performance. A joint design should be considered when integrating the two techniques together. Moreover, as RIS comprises only nearly passive elements, and accurate channel state information (CSI) for the RIS-related channels is hard to obtain [18]. Meanwhile, RS has been shown to be robust to CSI uncertainties [19]. Therefore RS is a good fit for RIS systems towards channel uncertainties [20].

Before the integration of RS and RIS, the joint design of RIS with other multiple access technologies has already been studied. In SDMA, the base station (BS) employs different linear precoding to serve different users simultaneously in the same frequency band for the downlink/uplink transmissions. Ref. [21] shows that conventional zero-forcing (ZF)

T. Zhang is with Ericsson Inc., Santa Clara, CA 95054. S. Mao is with the Department of Electrical and Computer Engineering, Auburn University, Auburn, AL 36849-5201, USA. Email: tzz0031@auburn.edu, smao@ieee.org.

This work was supported in part by the NSF under Grant ECCS-1923717, and the Wireless Engineering Research and Education Center at Auburn University, Auburn, AL, USA.

DOI: 10.1109/TWC.2023.3277334

beamforming is insufficient to null/suppress the interference from other users while a RIS can provide spatial interference nulling/cancellation capability to solve this problem. Compared with SDMA where interfering signals from other users are treated as noise, (power domain) NOMA allows users to be in the same time-frequency resource block and distinguishes them in the power domain. By doing so, NOMA has been regarded as a multiple access candidate technology to improve the system spectrum efficiency for future wireless networks [22]. The integration of RIS and NOMA has been shown to provide a cost-effective solution to achieve high energy efficiency [23], spectrum efficiency [24], and increased coverage [25]. Another multiple access technology, RS, has been shown in [9] to outperform and unify SDMA and NOMA under a wide range of network loads and user deployment. Despite its appealing advantages and a good fit with RIS technology, few technical contributions have been presented and the full possibilities of the integration of RIS and RS remain to be explored.

The RS beamforming design has been extensively studied. In [10], a sum rate maximization beamforming was studied with the weighted minimum mean squared error (WMMSE) method. In [26], a difference of convex functions (DC) programming was proposed to optimize the precoder covariance matrix. Secure and robust RS beamforming design was studied in [27] and [28] under imperfect CSI, respectively. Most of the previous works find a suboptimal solution with optimization techniques. Recently, global optimal beamforming was proposed in [29] to optimize the energy efficiency in an RS system with a branch and bound algorithm.

In terms of the joint beamforming design between RIS and RS, the authors in [30] explored the joint optimization in a RIS-assisted RS system. The successive convex approximation and semidefinite programming (SDP) is used to maximize the minimum rate of all users. This technique can return a rank-one solution for the RIS-assisted NOMA system [31]. However, this technique could not be extended to a RIS-assisted RS system since the rank-one condition may not be satisfied in an RS system [32]. Ref. [16] explores the on-off control for passive beamforming at the RIS. A closed-form expression for the outage probability for the cell-edge users is derived. Ref. [13] performs beamforming design to maximize the energy efficiency in a RIS-assisted RS system. Ref. [15] performs beamforming and RIS scatter matrix design to maximize the system's spectral efficiency. However, the above works all assume perfect CSI setting, which is unrealistic in practice. The mechanism and advantages of RS in combating the RIS-related channel uncertainties have not yet been studied so far.

This paper tries to develop novel and efficient beamforming algorithms for RIS-assisted RS systems and explore the interplay between RIS and RS in the imperfect CSI case. The main contribution of this paper is summarized as follows:

1) We formulate a max-min rate optimization problem to explore the interplay between RIS and RS techniques. The joint beamforming design is considered under different RIS configurations.
2) We employ the weighted mean squared error minimization (WMMSE) algorithm to transform the non-convex max-min rate problem into a more tractable form. A block coordination descent (BCD) algorithm is proposed to optimize the variables in an alternative manner. The algorithm was extended to the imperfect CSI case to explore the robustness of RS in combating RIS-related channel uncertainties.
3) We provide analysis on the impact of the system parameters. Numerical results show that RIS-assisted RS is robust towards channel uncertainties and outperforms the conventional multiple access technologies with/without RIS in terms of the max-min rate.

The remainder of this paper is organized as follows. Section II presents the system model and formulates the max-min rate maximization problem. Section III introduces a rate-WMMSE relationship, based on which a BCD algorithm is developed for different RIS setups. The algorithm is extended to the imperfect CSI case in Section IV. Numerical results are provided in Section V to evaluate the effectiveness of the proposed algorithms. Finally, Section VI concludes this paper.

Notation: The notation used in this paper is summarized as follows. Bold lower or upper case letters are used to denote vectors and matrices, respectively. $\mathcal{CN}(\mu, \sigma^2)$ denotes the circularly symmetric complex Gaussian distribution with mean μ and variance σ^2. For any scalar a, $|a|$ denotes the absolute value. For any vector $\mathbf{a}$, a_i is the ith element, and $\mathbf{a}^H$ represents its conjugate transpose. $\mathrm{Diag}(\mathbf{A})$ stands for a vector whose elements are extracted from the diagonal of matrix $\mathbf{A}$. $\mathrm{Rank}(\mathbf{A})$ denotes the rank of matrix $\mathbf{A}$. Variables with stars are optimal solutions.

II. System Model and Problem Formulation

A. System Model

The differences between RIS-assisted RS, NOMA, and SDMA are illustrated in Fig. 1. The figure shows a two-user system where the BS aims to deliver message s_1 to User 1 and message s_2 to User 2. In the SDMA system, each user treats the signal from other users as interference, as shown in Fig. 1(a). In the NOMA system, User 1 completely decodes the message from User 2 using successive interference cancellation (SIC), hence an improved spectrum efficiency can be achieved. Unlike NOMA and SDMA, the RS system shown in Fig. 1(c) generates messages using a public codebook known to all users. Each user partially decodes the messages for other users and partially treats the messages from other users as interference.

Specifically, we consider a downlink multi-user multiple-input-single-output (MISO) communication system, which consists of a BS with M antennas, and K user equipments (UEs) each with a single antenna, denoted by $\mathcal{K} = \{1, 2, ..., K\}$ [6], [10]. In RS, the message X_k intended for UE k is split into a private part $X_{\mathrm{p},k}$ and a common part $X_{\mathrm{c},k}$. The private parts are encoded independently into Gaussian data symbol streams, denoted as $[s_1, s_2, ..., s_k]^T \in \mathbb{C}^{K\times 1}$. Meanwhile, the common parts of all UEs $\{X_{\mathrm{c},1}, X_{\mathrm{c},2}, ..., X_{\mathrm{c},K}\}$ are combined into a common message X_{c}, which is encoded into a common stream s_{c} with a public codebook

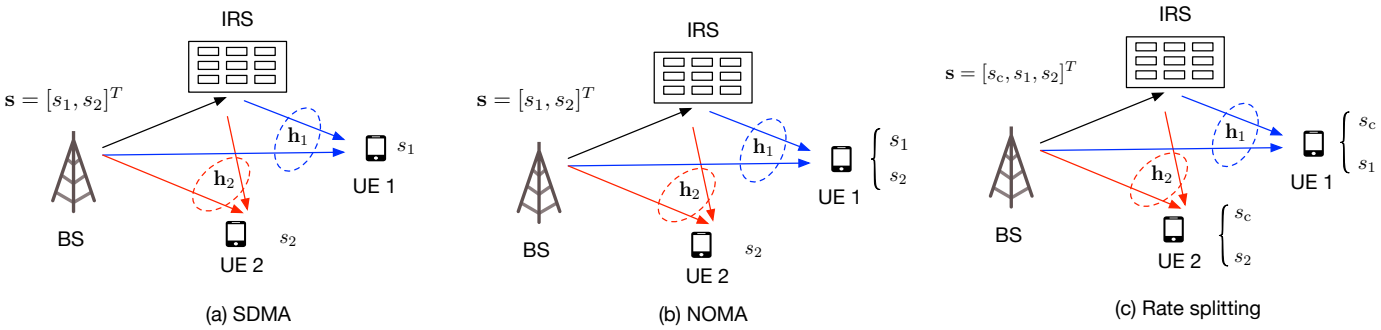

Fig. 1: Three multiple access technologies assisted by RIS: (a) SDMA, (b) NOMA, and (c) RS.

known to all UEs. As a result, the combined symbols are grouped into a vector $\mathbf{s} = [s_c, s_1, s_2, ..., s_K]^T \in \mathbb{C}^{(K+1)\times 1}$. Each signal is assumed to have zero mean and unit variance, i.e., $\mathbb{E}[\mathbf{s}\mathbf{s}^H] = \mathbf{I}_{K+1}$. At the transmitter, the precoding matrix for all UEs is $\mathbf{w} = [\mathbf{w}_c, \mathbf{w}_1, \mathbf{w}_2, ..., \mathbf{w}_K]$, where $\mathbf{w}_k \in \mathbb{C}^{M\times 1}$ is the precoding matrix for UE $k \in \mathcal{K}$ for its private data s_k, and $\mathbf{w}_c \in \mathbb{C}^{M\times 1}$ is the precoding matrix for the common message s_c.

To assist signal transmission, a RIS with N reflecting elements is placed between the UEs and the BS. The equivalent channels from the BS to UE k, from the RIS to UE k, and from the BS to the RIS are denoted as $\mathbf{h}_{d,k} \in \mathbb{C}^{M\times 1}$, $\mathbf{h}_{r,k} \in \mathbb{C}^{N\times 1}$, and $\mathbf{G} \in \mathbb{C}^{N\times M}$, respectively. The combined channel between the BS and UE k, $\mathbf{h}_k \in \mathbb{C}^{M\times 1}$, can be regarded as a combination of the direct and the reflected channels, i.e.,

$$\mathbf{h}_k \triangleq \mathbf{h}_{d,k} + \mathbf{G}^H \mathbf{\Theta} \mathbf{h}_{r,k}, \tag{1}$$

where $\mathbf{\Theta} \in \mathbb{C}^{N\times N}$ is the RIS phase shift matrix. Note that the RIS reflection phase-shift matrix $\mathbf{\Theta}$ is a diagonal matrix with diagonal elements $v_i = \beta_i e^{j\theta_i}$, where $\theta_i \in [0, 2\pi]$ and $\beta_i \in [0, 1]$, $1 \le i \le N$. We extract the diagonal elements of $\mathbf{\Theta}$ and let $\mathbf{v} = \text{diag}\{\mathbf{\Theta}\} \in \mathbb{C}^{N\times 1}$. Then we have $\mathbf{h}_k = \mathbf{h}_{d,k} + \mathbf{H}_k^H \mathbf{v}$, where $\mathbf{H}_k = \text{diag}\{\mathbf{h}_{r,k}^H\}\mathbf{G} \in \mathbb{C}^{N\times M}$. The reflection matrix $\mathbf{\Theta}$ captures the effective phase shifts of all the reflecting elements on the RIS. The phase shift unit can be adjusted by the RIS controller based on measured channel dynamics. Depending on the amplitude and phase shift of the reflecting elements, we consider two types of RIS in this paper [31].

- RIS Φ_1 : the reflecting elements can be adjusted with arbitrary continuous amplitudes and phase, i.e., $\Phi_1 = \{\beta_i e^{j\theta_i} | \theta_i \in [0, 2\pi], \beta_i \in [0, 1]\}$.
- RIS Φ_2: The reflection amplitude is fixed and only the phase can be adjusted. If the phase can be adjusted continuously, the feasible set is expressed as $\Phi_2 = \{e^{j\theta_i} | \theta_i \in [0, 2\pi]\}$. This setting can be extended to a quantized phase shift.

The received signal for UE k can be expressed as

$$y_k = \mathbf{h}_k^H \sum_{i\in\mathcal{M}} \mathbf{w}_i s_i + n_k, \quad \forall k \in \mathcal{K}, \tag{2}$$

where $\mathcal{M} = \mathcal{K} \cup \{c\}$ denotes the combined set and $n_k \sim \mathcal{CN}(0, \sigma_0^2)$ is the additive white Gaussian noise at UE k.

At the receiver, each UE first decodes the common stream by treating all the private streams as noise. Then its private message is decoded by removing the decoded common stream with SIC. After the decoding process, the receiver recombines messages into original messages. The decoding SINR for the common message and the private message for UE k at the receiver is given by

$$\gamma_{c,k} = \frac{|\mathbf{h}_k^H \mathbf{w}_c|^2}{\sum_{i\in\mathcal{K}} |\mathbf{h}_k^H \mathbf{w}_i|^2 + \sigma_0^2}, \quad \forall k \in \mathcal{K}, \tag{3}$$

$$\gamma_{p,k} = \frac{|\mathbf{h}_k^H \mathbf{w}_k|^2}{\sum_{i\in\mathcal{K}, i\neq k} |\mathbf{h}_k^H \mathbf{w}_i|^2 + \sigma_0^2}, \quad \forall k \in \mathcal{K}. \tag{4}$$

Under Gaussian signaling, the achievable rate of UE k in decoding the common rate and the private rate are given by

$$r_{c,k} = \log_2(1 + \gamma_{c,k}), \quad R_{p,k} = \log_2(1 + \gamma_{p,k}). \tag{5}$$

To ensure that all UEs can decode the common message stream, the actual rate of the common message stream, denote as r_c, is constrained by each $r_{c,k}$, i.e.,

$$r_c = \min_{k\in\mathcal{K}} r_{c,k}. \tag{6}$$

According to the RS decoding principle, the actual data stream r_c is shared by all UEs. By denoting $R_{c,k}$ as the general common rate allocated to UE k, we have

$$\sum_{k\in\mathcal{K}} R_{c,k} \le r_c, \quad R_{c,k} \ge 0. \tag{7}$$

After removing the common data stream, each UE decodes its own private message. Finally, the overall achievable data rate for UE k is given by

$$R_k = R_{c,k} + R_{p,k}, \quad \forall k \in \mathcal{K}. \tag{8}$$

B. Problem Formulation

In this paper, we aim to maximize the minimum achievable rate of all UEs by jointly performing active beamforming at the BS as well as passive beamforming at the RIS. Specifically,

the problem can be mathematically formulated as

$$\max_{\mathbf{w},\mathbf{R}_{\rm c},\mathbf{R}_{\rm p},\mathbf{v},s} \quad s \tag{9a}$$

$$\text{s.t.} \quad \sum_{k\in\mathcal{M}} ||\mathbf{w}_k||^2 \le P \tag{9b}$$

$$v_i \in \Phi,\ \forall i \tag{9c}$$

$$R_{{\rm p},k} + R_{{\rm c},k} \ge s \tag{9d}$$

$$R_{{\rm p},k} \le \log_2(1+\gamma_{{\rm p},k}),\ \forall k \tag{9e}$$

$$\sum_{k\in\mathcal{K}} R_{{\rm c},k} \le \log_2(1+\gamma_{{\rm c},k}),\ \forall k, \tag{9f}$$

where $\mathbf{w} = \{\mathbf{w}_i | i \in \mathcal{M}\}$, $\mathbf{R}_{\rm p} = \{R_{{\rm p},k} | k \in \mathcal{K}\}$, $\mathbf{R}_{\rm c} = \{R_{{\rm c},k} | k \in \mathcal{K}\}$, P is the total transmit power at the BS, and Φ denotes one of the set in Φ_1 or Φ_2.

The formulated problem is non-convex optimization where the non-convexity is due to $R_{{\rm p},k}$ and $R_{{\rm c},k}$. As can be seen from (5), the expression of $R_{{\rm p},k}$ involves the logarithmic operation of $\gamma_{{\rm p},k}$, which is concave. The inner function $\gamma_{{\rm p},k}$, as shown in (3), involves a quadratic-over-linear operation of $\mathbf{w}$, which is convex. As a result, the combined expression of $R_{{\rm p},k}$ is neither concave nor convex. Moreover, the beamforming vector $\mathbf{w}$ is coupled with the RIS phase shift matrix $\mathbf{\Theta}$, which makes the problem more challenging.

III. Joint Beamforming Design with Perfect CSI

It can be seen that Problem (9) is a joint beamforming design problem, which is to find the active beamforming $\mathbf{w}$ at the BS as well as the passive beamforming $\mathbf{\Theta}$ at the RIS. To deal with the coupling between the passive beamforming and the active beamforming, we propose to use the alternative optimization (AO) framework, which optimizes the active beamforming and the passive beamforming iteratively.

A. The BCD-based Approach for RIS: Φ_1

Refs. [5], [7], [10] have proposed a weighted minimum mean square error (WMMSE) approach to solve this problem. The WMMSE method utilizes the relationship between mutual information and MMSE to find a stationary solution. Let the estimated common message of UE k be denoted as $\hat{s}_{{\rm c},k} = g_{{\rm c},k} y_k$ with $g_{{\rm c},k}$ being a scalar equalizer. Then an estimate of s_k can be expressed as $\hat{s}_k = g_{{\rm p},k}(y_k - \mathbf{h}_k^H \mathbf{w}_{\rm c} s_{{\rm c},k})$, since the interference from the common message can be removed at each UE. Then, the mean-squared errors (MSE) of the common message and the private message can be expressed respectively as

$$\epsilon_{{\rm c},k} = \mathbb{E}[|\hat{s}_{{\rm c},k} - s_{{\rm c},k}|^2] = |g_{{\rm c},k}|^2 T_{{\rm c},k} - 2{\rm Re}(g_{{\rm c},k}\mathbf{h}_k^H \mathbf{w}_{\rm c}) + 1, \tag{10}$$

$$\epsilon_{{\rm p},k} = \mathbb{E}[|\hat{s}_k - s_k|^2] = |g_{{\rm p},k}|^2 T_{{\rm p},k} - 2{\rm Re}(g_{{\rm p},k}\mathbf{h}_k^H \mathbf{w}_k) + 1, \tag{11}$$

where

$$T_{{\rm c},k} = \mathbb{E}[|y_k|^2] = \sum_{i\in\mathcal{M}} |\mathbf{h}_k^H \mathbf{w}_i|^2 + \sigma_0^2,$$

$$T_{{\rm p},k} = \mathbb{E}[|y_k|^2] - |\mathbf{h}_k^H \mathbf{w}_{\rm c}|^2 = \sum_{i\in\mathcal{K}} |\mathbf{h}_k^H \mathbf{w}_i|^2 + \sigma_0^2.$$

To minimize the MSE of both the common and the private messages, we take the derivative of the MSE in (10) w.r.t. the scalar equalizer, i.e., $\partial\epsilon_{{\rm c},k}/\partial g_{{\rm c},k} = 0$ and $\partial\epsilon_{{\rm p},k}/\partial g_{{\rm p},k} = 0$. Then we obtain the optimal MMSE equalizer as

$$g_{{\rm c},k}^{\rm MMSE} = \mathbf{h}_k^H \mathbf{w}_{\rm c}/T_{{\rm c},k}, \quad g_{{\rm p},k}^{\rm MMSE} = \mathbf{h}_k^H \mathbf{w}_k/T_{{\rm p},k}. \tag{13}$$

Substituting the optimal equalizer (13) into the MSE (10), we obtain the minimum MSE as

$$\epsilon_{{\rm c},k}^{\rm MMSE} = 1 - \frac{|\mathbf{h}_k^H \mathbf{w}_{\rm c}|^2}{T_{{\rm c},k}}, \quad \epsilon_{{\rm p},k}^{\rm MMSE} = 1 - \frac{|\mathbf{h}_k^H \mathbf{w}_k|^2}{T_{{\rm p},k}}. \tag{14}$$

By comparing (14) with (3) and (5), we obtain the rate-MMSE relationship as

$$r_{{\rm c},k} = -\log_2(\epsilon_{{\rm c},k}^{\rm MMSE}), \quad R_{{\rm p},k} = -\log_2(\epsilon_k^{\rm MMSE}). \tag{15}$$

Meanwhile, the augmented weighted MSE (WMSE) can be defined as

$$\xi_{{\rm c},k} = u_{{\rm c},k}\epsilon_{{\rm c},k}^{\rm MMSE} - \ln(u_{{\rm c},k}), \tag{16a}$$

$$\xi_{{\rm p},k} = u_{{\rm p},k}\epsilon_{{\rm p},k}^{\rm MMSE} - \ln(u_{{\rm p},k}), \tag{16b}$$

where $u_{{\rm c},k} > 0$ and $u_{{\rm p},k} > 0$ are the associated weights with UE k's MSE. The weighted MMSE (WMMSE) is defined as the minimum augmented WMSE over all possible weights, i.e., $\xi_{{\rm c},k}^{\rm MMSE} = \min_{u_{{\rm c},k}} \xi_{{\rm c},k}$ and $\xi_{{\rm p},k}^{\rm MMSE} = \min_{u_{{\rm p},k}} \xi_{{\rm p},k}$. Now we take derivative w.r.t. the weights in (16), i.e., $\partial\xi_{{\rm c},k}/\partial u_{{\rm c},k} = 0$ and $\partial\xi_{{\rm p},k}/\partial u_{{\rm p},k} = 0$. Then we obtain the optimal weight as

$$u_{{\rm c},k}^{\rm MMSE} = \frac{1}{\epsilon_{{\rm c},k}^{\rm MMSE}}, \quad u_{{\rm p},k}^{\rm MMSE} = \frac{1}{\epsilon_{{\rm p},k}^{\rm MMSE}}. \tag{17}$$

Combining (15), (16) and (17)), we obtain the rate-WMMSE relationship as

$$\xi_{{\rm c},k}^{\rm MMSE} = 1 + \ln\left(\epsilon_{{\rm c},k}^{\rm MMSE}\right) = 1 - r_{{\rm c},k}\ln 2, \tag{18a}$$

$$\xi_{{\rm p},k}^{\rm MMSE} = 1 + \ln\left(\epsilon_{{\rm p},k}^{\rm MMSE}\right) = 1 - R_{{\rm p},k}\ln 2. \tag{18b}$$

This will be the core relationship in the WMMSE algorithm.

With the rate-WMMSE relationship (18), the max-min rate problem in (9) can be equivalently rewritten as

$$\max_{\mathbf{w},\mathbf{G},\mathbf{U},s,\mathbf{R}_{\rm c},\mathbf{R}_{\rm p},\mathbf{v}} \quad s \tag{19a}$$

$$\text{s.t.} \quad \frac{1-\xi_{{\rm c},k}}{\ln 2} \ge \sum_{k\in\mathcal{K}} R_{{\rm c},k} \tag{19b}$$

$$\frac{1-\xi_{{\rm p},k}}{\ln 2} \ge R_{{\rm p},k} \tag{19c}$$

$$R_{{\rm c},k} + R_{{\rm p},k} \ge s \tag{19d}$$

$$v_i \in \Phi_1,\ \forall i \tag{19e}$$

$$(9b), (7),$$

where $\mathbf{G} = \{g_{{\rm c},k}, g_{{\rm p},k} | k \in \mathcal{K}\}$ are the sets of scalar equalizers, $\mathbf{U} = \{u_{{\rm c},k}, u_{{\rm p},k} | k \in \mathcal{K}\}$ is the set of associated weights of UEs' MSE, and $\xi_{{\rm c},k}$ and $\xi_{{\rm p},k}$ are given in (16).

Theorem 1. *The stationary solution to Problem (19) that satisfies conditions (13) and (17) is also a stationary solution to Problem (9).*

Proof. We refer readers to [7] for detailed proof. □

Substituting $\mathbf{h}_k = \mathbf{h}_{\mathrm{d},k} + \mathbf{H}_k^H \mathbf{v}$ into (12), we have

$$T_{\mathrm{c},k} = \mathbf{v}^H \mathbf{Q}_{\mathrm{c},k} \mathbf{v} + 2\mathrm{Re}\left(\mathbf{v}^H \mathbf{q}_{\mathrm{c},k}\right) + \alpha_{\mathrm{c},k} + \sigma_0^2,$$
$$T_{\mathrm{p},k} = \mathbf{v}^H \mathbf{Q}_{\mathrm{p},k} \mathbf{v} + 2\mathrm{Re}\left(\mathbf{v}^H \mathbf{q}_{\mathrm{p},k}\right) + \alpha_{\mathrm{p},k} + \sigma_0^2,$$

where $\mathbf{Q}_{\mathrm{c},k} = \sum_{i\in\mathcal{M}} \mathbf{H}_k \mathbf{w}_i \mathbf{w}_i^H \mathbf{H}_k^H$, $\mathbf{q}_{\mathrm{c},k} = \sum_{i\in\mathcal{M}} \mathbf{H}_k \mathbf{w}_i \mathbf{w}_i^H \mathbf{h}_{\mathrm{d},k}$, $\alpha_{\mathrm{c},k} = \sum_{i\in\mathcal{M}} |\mathbf{h}_{\mathrm{d},k}^H \mathbf{w}_i|^2$, $\mathbf{Q}_{\mathrm{p},k} = \sum_{i\in\mathcal{K}} \mathbf{H}_k \mathbf{w}_i \mathbf{w}_i^H \mathbf{H}_k^H$, $\mathbf{q}_{\mathrm{p},k} = \sum_{i\in\mathcal{K}} \mathbf{H}_k \mathbf{w}_i \mathbf{w}_i^H \mathbf{h}_{\mathrm{d},k}$, and $\alpha_{\mathrm{p},k} = \sum_{i\in\mathcal{K}} |\mathbf{h}_{\mathrm{d},k}^H \mathbf{w}_i|^2$.

Although Problem (19) is till non-convex, it has a block-wise convex property w.r.t. $\mathbf{w}$, $(\mathbf{G}, \mathbf{U})$, and $\mathbf{v}$. When $\mathbf{w}$ and $\mathbf{v}$ are fixed, the problem is convex w.r.t. $(\mathbf{G}, \mathbf{U})$. When $\mathbf{v}$ and $(\mathbf{G}, \mathbf{U})$ are fixed, we will obtain $\xi_{\mathrm{c},k}$ and $\xi_{\mathrm{p},k}$ as shown in (22), which is a second-order cone in terms of $\mathbf{w}$. When $\mathbf{w}$ and $(\mathbf{G}, \mathbf{U})$ are fixed, we obtain $\xi_{\mathrm{c},k}$ and $\xi_{\mathrm{p},k}$ as shown in (23), which is also a second-order cone in terms of $\mathbf{v}$. Hence the block coordinate descent (BCD) method, which successively optimizes each of the variables, can be used. The details of the BCD algorithm are as follows.

1) *The optimization of* $(\mathbf{G}, \mathbf{U})$*:* The scaling factor $\mathbf{G}$ and the optimal weight $\mathbf{U}$ have closed-form expressions, which are given in (13) and (17), respectively.
2) *The optimization of* $\mathbf{w}$*:* The optimal $\mathbf{w}$ can be obtained by solving the following problem.

$$\max_{\mathbf{w},s,\mathbf{R}_{\mathrm{c}},\mathbf{R}_{\mathrm{p}}} \quad s \tag{20}$$
$$\text{s.t.} \quad (19b),\ (19c),\ (19d),\ (9b), (7),$$

where $\xi_{\mathrm{c},k}$ and $\xi_{\mathrm{p},k}$ are given in (22).
3) *The optimization of* $\mathbf{v}$*:* The optimal $\mathbf{v}$ can be obtained by solving the following problem.

$$\max_{\mathbf{v},s,\mathbf{R}_{\mathrm{c}},\mathbf{R}_{\mathrm{u}}} \quad s \tag{21}$$
$$\text{s.t.} \quad (19b),\ (19c),\ (19d),\ (7),$$
$$|v_i|^2 \le 1, \forall i.$$

where $\xi_{\mathrm{c},k}$ and $\xi_{\mathrm{p},k}$ are given in (23).

To summarize, the proposed algorithm successively optimizes the variables. Its complexity mainly comes from Step 2 and Step 3, which are two quadratically constrained convex optimization problems (QCCP). The QCCP problem in Step 2 consists of $d_1 = 4K + 2$ constraints and $d_2 = 1 + 2K + MK$ variables. Hence, the worst case computational complexity of solving this problem is $\mathcal{O}(d_1 d_2^2 + d_2^3)\sqrt{d_1}\log(1/\epsilon)$ [33] for a given stopping criterion ϵ. Similarly, the problem in Step 3 is also a QCCP, which has $d_3 = 4K + 1$ constraints and $d_4 = 1 + 2K + N^2$ variables. The computational complexity in Step 3 is $\mathcal{O}(d_3 d_4^2 + d_4^3)\sqrt{d_3}\log(1/\epsilon)$. Hence, the overall complexity of the BCD algorithm is $\mathcal{O}(I_{\mathrm{in}}(M^3 K^{3.5} + (K + N^2)^3 K^{0.5})\log(1/\epsilon))$, where I_{in} is the total number of outer iterations of the BCD algorithm.

Theorem 2. *The proposed BCD algorithm will converge after a finite amount of steps.*

Proof. Denote the objective function in (19) as $F(\mathbf{G}, \mathbf{U}, \mathbf{w}, \mathbf{v})$. Then we have

$$F(\mathbf{G}^{t-1}, \mathbf{U}^{t-1}, \mathbf{w}^t, \mathbf{v}^t) \le F(\mathbf{G}^t, \mathbf{U}^t, \mathbf{w}^t, \mathbf{v}^t)$$
$$\le F(\mathbf{G}^t, \mathbf{U}^t, \mathbf{w}^{t+1}, \mathbf{v}^t) \le F(\mathbf{G}^t, \mathbf{U}^t, \mathbf{w}^{t+1}, \mathbf{v}^{t+1}),$$

where the first inequality holds since $\mathbf{U}^t$ is the optimal weight and $\mathbf{G}^t$ is the optimal MMSE equalizer to minimize the MSE. The second inequality holds since $\mathbf{w}^{t+1}$ is the optimal solution to Problem (20) and the third inequality holds since $\mathbf{v}^{t+1}$ is the optimal solution to Problem (21). □

B. The Penalty-based BCD Approach for RIS:Φ_2

In the RIS:Φ_2 case, we need to deal with the non-convex constraints with Φ_2. The problem becomes

$$\max_{\mathbf{w},\mathbf{G},\mathbf{U},s,\mathbf{R}_{\mathrm{c}},\mathbf{R}_{\mathrm{p}},\mathbf{v}} \quad s, \tag{24a}$$
$$\text{s.t.} \quad (19b),\ (19c),\ (19d),\ (9b), (7)$$
$$v_i \in \Phi_2,\ \forall i. \tag{24b}$$

To simplify the optimization of $\mathbf{v}$ and facilitate parallel updating, we propose to use the penalty dual decomposition (PDD) framework. This method introduces an auxiliary variable $\mathbf{u}$. Hence Problem (24) is equivalently transformed to

$$\max_{\mathbf{w},\mathbf{G},\mathbf{U},s,\mathbf{R}_{\mathrm{c}},\mathbf{R}_{\mathrm{p}},\mathbf{v}} \quad s \tag{25a}$$
$$\text{s.t.} \quad (19b),\ (19c),\ (19d),\ (9b),\ (7)$$
$$\mathbf{v} = \mathbf{u}, \tag{25b}$$
$$u_i \in \Phi_2,\ \forall i. \tag{25c}$$

To deal with the constraint $\mathbf{v} = \mathbf{u}$, Problem (24) is further transformed to

$$\max_{\mathbf{w},\mathbf{G},\mathbf{U},s,\mathbf{R}_{\mathrm{c}},\mathbf{R}_{\mathrm{p}},\mathbf{v}} \quad z = s - \frac{1}{2\rho}||\mathbf{v} - \mathbf{u} + \rho\boldsymbol{\mu}||^2 \tag{26a}$$
$$\text{s.t.} \quad (19b),\ (19c),\ (19d),\ (9b),\ (7)$$
$$u_i \in \Phi_2,\ \forall i, \tag{26b}$$

where ρ is a penalty coefficient and $\boldsymbol{\mu}$ is the dual variable vector associated with constraint $\mathbf{v} = \mathbf{u}$. To optimize the variable vector $\mathbf{u}$, we solve the following sub-problem.

$$\min_{\mathbf{u}} \quad ||\mathbf{v} - \mathbf{u} + \rho\boldsymbol{\mu}||^2 \tag{27}$$
$$\text{s.t.} \quad u_i \in \Phi_2, \forall i. \tag{28}$$

For this problem, we notice that u_i is decoupled in both the objective function and the constraint. Hence we can obtain the optimal solution in parallel. Note that

$$||\mathbf{v} - \mathbf{u} + \rho\boldsymbol{\mu}||^2$$
$$= (\mathbf{v} + \rho\boldsymbol{\mu})^H(\mathbf{v} + \rho\boldsymbol{\mu}) + \mathbf{u}^H\mathbf{u} - 2\mathrm{Re}(\mathbf{u}^H(\mathbf{v} + \rho\boldsymbol{\mu})). \tag{29}$$

When $u_i \in \Phi_2$, we have $|u_i| = 1$. Hence $\mathbf{u}^H\mathbf{u} = N$. To minimize the term $||\mathbf{v} - \mathbf{u} + \rho\boldsymbol{\mu}||^2$, the phase of $\mathbf{u}$ and the phase of $\mathbf{v} + \rho\boldsymbol{\mu}$ should be the same, i.e.,

$$u_i = \exp\left\{j\angle\bar{v}_i\right\}, \tag{30}$$

where $\bar{v}_i$ is the element of $\bar{\mathbf{v}}$ and $\bar{\mathbf{v}} = \mathbf{v} + \rho\boldsymbol{\mu}$.

We design an iterative algorithm where the inner loop optimizes variables $(\mathbf{G}, \mathbf{U}, \mathbf{w}, \mathbf{v}, \mathbf{u})$ successively. In the outer loop, the dual variable ρ is decreased by a factor of α and the dual variable $\boldsymbol{\mu}$ is updated by

$$\boldsymbol{\mu} = \boldsymbol{\mu} + \frac{1}{\rho}(\mathbf{v} - \mathbf{u}). \tag{31}$$

$$\xi_{\mathrm{c},k}(\mathbf{w}) = u_{\mathrm{c},k}\left[|g_{\mathrm{c},k}|^2\left(\sum_{i\in\mathcal{M}}\mathbf{w}_i^H\mathbf{h}_k\mathbf{h}_k^H\mathbf{w}_i+\sigma_0^2\right)-2\mathrm{Re}(g_{\mathrm{c},k}\mathbf{h}_k^H\mathbf{w}_{\mathrm{c}})+1\right]-\ln(u_{\mathrm{c},k}), \tag{22a}$$

$$\xi_{\mathrm{p},k}(\mathbf{w}) = u_{\mathrm{p},k}\left[|g_{\mathrm{p},k}|^2\left(\sum_{i\in\mathcal{K}}\mathbf{w}_i^H\mathbf{h}_k\mathbf{h}_k^H\mathbf{w}_i+\sigma_0^2\right)-2\mathrm{Re}(g_{\mathrm{p},k}\mathbf{h}_k^H\mathbf{w}_k)+1\right]-\ln(u_{\mathrm{p},k}). \tag{22b}$$

$$\xi_{\mathrm{c},k}(\mathbf{v}) = u_{\mathrm{c},k}\left[|g_{\mathrm{c},k}|^2\left(\mathbf{v}^H\mathbf{Q}_{\mathrm{c},k}\mathbf{v}+2\mathrm{Re}\left(\mathbf{v}^H\mathbf{q}_{\mathrm{c},k}\right)+\alpha_{\mathrm{c},k}+\sigma_0^2\right)-2\mathrm{Re}(g_{\mathrm{c},k}\mathbf{h}_{\mathrm{d},k}^H\mathbf{w}_{\mathrm{c}}+g_{\mathrm{c},k}\mathbf{v}^H\mathbf{H}_k\mathbf{w}_{\mathrm{c}})+1\right]-\ln(u_{\mathrm{c},k}), \tag{23a}$$

$$\xi_{\mathrm{p},k}(\mathbf{v}) = u_{\mathrm{p},k}\left[|g_{\mathrm{p},k}|^2\left(\mathbf{v}^H\mathbf{Q}_{\mathrm{p},k}\mathbf{v}+2\mathrm{Re}\left(\mathbf{v}^H\mathbf{q}_{\mathrm{p},k}\right)+\alpha_{\mathrm{p},k}+\sigma_0^2\right)-2\mathrm{Re}(g_{\mathrm{p},k}\mathbf{h}_{\mathrm{d},k}^H\mathbf{w}_k+g_{\mathrm{p},k}\mathbf{v}^H\mathbf{H}_k\mathbf{w}_k)+1\right]-\ln(u_{\mathrm{p},k}). \tag{23b}$$

As can be seen, algorithm 1 consists of an outer loop that decreases the penalty factor and an inner loop that optimizes the variables successively. With the decrease of the penalty coefficient, the penalty term becomes larger and will eventually guarantee that $\mathbf{u} = \mathbf{v}$. For the inner loop, the complexity is the same as that of the BCD algorithm. Steps 11 and 12 in the outer loop also have closed-form expressions. We conclude that the overall complexity of Algorithm 1 is $\mathcal{O}(I_{\mathrm{out}}I_{\mathrm{in}}(M^3K^{3.5}+(K+N^2)^3K^{0.5})\log(1/\epsilon))$.

Algorithm 1 Penalty-based BCD Algorithm

Input: P;
Output: $\mathbf{w}^*$, $\mathbf{v}^*$;

1: Initialize outer loop iteration index $I_{\mathrm{out}}=0$; Initialize the beamforming vector with equal power allocation $\frac{P}{M(K+1)}$; Generate vector $\mathbf{v}$ and $\mathbf{u}$ with reflection amplitude 1 and random phases; Initialize $\boldsymbol{\mu}=\mathbf{0}$ and $\rho=200$.
2: **repeat**
3: Initialize inner loop iteration index $I_{\mathrm{in}}=0$;
4: **repeat**
5: Update $\mathbf{G}^t$ and $\mathbf{U}^t$ based on (13) and (17);
6: Obtain $\mathbf{w}^{t+1}$ by solving convex optimization Problem (20);
7: Obtain $\mathbf{v}^{t+1}$ by solving Problem (26a);
8: Obtain $\mathbf{u}^{t+1}$ from (30) when $\Phi=\Phi_2$;
9: $I_{\mathrm{in}}++$;
10: **until** $\frac{|z^t-z^{t-1}|}{|z^{t-1}|}\geq\epsilon$ or $I_{\mathrm{in}}>I_{\mathrm{in}}^{\max}$
11: Update $\boldsymbol{\mu}$ based on (31);
12: Update ρ by $\rho=c\rho$;
13: $I_{\mathrm{out}}++$;
14: **until** $||\mathbf{u}-\mathbf{v}||_2\leq\epsilon$

IV. Joint beamforming design with imperfect CSI

In practice, joint beamforming design requires precise CSI, which is quite challenging to obtain. In this section, we consider the scenario where the users know the perfect CSI while the BS only has the imperfect CSI estimation due to feedback errors and mismatches.

We assume that the CSI error model is given by

$$\mathbf{H}_k = \hat{\mathbf{H}}_k + \Delta\mathbf{H}_k,$$
$$\mathbf{h}_{\mathrm{d},k} = \hat{\mathbf{h}}_{\mathrm{d},k} + \Delta\mathbf{h}_{\mathrm{d},k}$$

where $\hat{\mathbf{H}}_k$ and $\hat{\mathbf{h}}_{\mathrm{d},k}$ denote the estimated cascaded channel and the estimated direct channel, respectively. $\Delta\mathbf{H}_k$ and $\Delta\mathbf{h}_{\mathrm{d},k}$ denote the CSI error of the cascaded channel and the direct channel, respectively. It is shown in [34] that when the number of the reflecting elements on the RIS is large, the distribution of $\mathrm{vec}(\Delta\mathbf{H}_k)$ is approximated by Gaussian distribution. In the rest of this paper, we assume that $\mathrm{vec}(\Delta\mathbf{H}_k)\sim\mathcal{CN}(\mathbf{0},\sigma_{\Delta H,k}^2\mathbf{I})$ and $\Delta\mathbf{h}_{\mathrm{d},k}\sim\mathcal{CN}(\mathbf{0},\sigma_{\Delta\mathrm{d},k}^2\mathbf{I})$. Moreover, the CSI error variances decay at a speed proportional to the channel variances, i.e., $\sigma_{\Delta\mathrm{d},k}^2=\frac{\delta}{M}||\mathbf{h}_{\mathrm{d},k}||^2$ and $\sigma_{\Delta H,k}^2=\frac{\delta}{MN}||\mathbf{H}_k||_F^2$ where $\delta\in[0,1]$ measures the relative CSIT uncertainties [35], [36].

The BS is assumed to know the the estimated channel $\hat{\mathbf{h}}_k=\hat{\mathbf{h}}_{\mathrm{d},k}+\hat{\mathbf{H}}_k^H\mathbf{v}$ and the conditional probability $p_{\mathbf{h}_k|\hat{\mathbf{h}}_k}(\mathbf{h}_k|\hat{\mathbf{h}}_k)$. According to [10], we can formulate the average rate (AR) optimization problem

$$\max_{\mathbf{w},\mathbf{R}_{\mathrm{c}},\mathbf{R}_{\mathrm{p}},\mathbf{v},s} \quad s \tag{32a}$$
$$\text{s.t.} \quad (9b),(9c) \tag{32b}$$
$$R_{\mathrm{p},k}+R_{\mathrm{c},k}\geq s \tag{32c}$$
$$R_{\mathrm{p},k}\leq\mathbb{E}_{\mathbf{h}_k|\hat{\mathbf{h}}_k}[\log_2(1+\gamma_{\mathrm{p},k})|\hat{\mathbf{h}}_k],\ \forall k \tag{32d}$$
$$\sum_{k\in\mathcal{K}}R_{\mathrm{c},k}\leq\mathbb{E}_{\mathbf{h}_k|\hat{\mathbf{h}}_k}[\log_2(1+\gamma_{\mathrm{c},k})|\hat{\mathbf{h}}_k],\ \forall k, \tag{32e}$$

To deal with the challenging stochastic optimization problem, we resort to the sample average approximation (SAA) method, which approximates the stochastic problem with a deterministic one. To be specific, for a given channel estimate $\hat{\mathbf{h}}_k$, we use set $\mathbb{H}^L$ to denote L i.i.d. channel realizations drawn from the conditional distribution $f_{\mathbf{h}_k|\hat{\mathbf{h}}_k}(\mathbf{h}_k|\hat{\mathbf{h}}_k)$.

$$\mathbb{H}^L=\{\mathbf{h}_k^l=\hat{\mathbf{h}}_k+\Delta\mathbf{h}_k^l|\hat{\mathbf{h}}_k,1\leq l\leq L,k\in\mathcal{K}\} \tag{33}$$

It was proven in [10] that when the sample size L is large enough, the stochastic rate can be approximated by the sample average. Hence if we define the sample average as

$$\bar{R}_{\mathrm{p},k}=\frac{1}{L}\sum_{l=1}^{L}R_{\mathrm{p},k}^l,\qquad \bar{R}_{\mathrm{c},k}=\frac{1}{L}\sum_{l=1}^{L}R_{\mathrm{c},k}^l$$

where $R_{\mathrm{p},k}^l$ and $R_{\mathrm{c},k}^l$ are the private rate and common rate associated with the channel realization $\{\mathbf{h}_k^l\}_k$. This leads to

the SAA problem

$$\max_{\mathbf{w},\bar{\mathbf{R}}_{\rm c},\bar{\mathbf{R}}_{\rm p},\mathbf{v},s} \quad s \tag{34a}$$

$$\text{s.t.} \quad (9b),(9c) \tag{34b}$$

$$\bar{R}_{{\rm p},k}+\bar{R}_{{\rm c},k}\geq s \tag{34c}$$

$$\bar{R}_{{\rm p},k}\leq \frac{1}{L}\sum_{l=1}^{L}\log_2(1+\gamma_{{\rm p},k}^{l}),\ \forall k \tag{34d}$$

$$\sum_{k\in\mathcal{K}}\bar{R}_{{\rm c},k}\leq \frac{1}{L}\sum_{l=1}^{L}\log_2(1+\gamma_{{\rm c},k}^{l}),\ \forall k, \tag{34e}$$

where $\bar{\mathbf{R}}_{\rm p}=\{\bar{R}_{{\rm p},k}|k\in\mathcal{K}\}$, $\bar{\mathbf{R}}_{\rm c}=\{\bar{R}_{{\rm c},k}|k\in\mathcal{K}\}$, and $\gamma_{{\rm p},k}^{l}$ and $\gamma_{{\rm c},k}^{l}$ are the associated SINR with the channel realization $\mathbf{h}_k^l$. In the optimization process, the same beamforming vector $\mathbf{w}$ is fixed for all the channel realizations.

Although this problem is deterministic, it is still non-convex. Following a similar step in section III, we approximate

$$\mathbb{E}_{\mathbf{h}_k|\hat{\mathbf{h}}_k}[\min_{u_{{\rm c},k}}\xi_{{\rm c},k}|\hat{\mathbf{h}}_k]\approx\min_{u_{{\rm c},k}}\bar{\xi}_{{\rm c},k}=\bar{\xi}_{{\rm c},k}^{\rm MMSE}=1-\bar{r}_{{\rm c},k}\ln 2$$

$$\mathbb{E}_{\mathbf{h}_k|\hat{\mathbf{h}}_k}[\min_{u_{{\rm p},k}}\xi_{{\rm p},k}|\hat{\mathbf{h}}_k]\approx\min_{u_{{\rm p},k}}\bar{\xi}_{{\rm p},k}=\bar{\xi}_{{\rm p},k}^{\rm MMSE}=1-\bar{R}_{{\rm p},k}\ln 2$$

where $\bar{r}_{{\rm c},k}=\frac{1}{L}\sum_{l=1}^{L}\log_2(1+\gamma_{{\rm c},k}^{l})$. With this relationship, the SAA max-min rate problem (34) can be equivalently transformed into

$$\max_{\mathbf{w},\bar{\mathbf{G}},\bar{\mathbf{U}},s,\bar{\mathbf{R}}_{\rm c},\bar{\mathbf{R}}_{\rm p},\mathbf{v}} \quad s \tag{35a}$$

$$\text{s.t.} \quad \frac{1-\bar{\xi}_{{\rm c},k}}{\ln 2}\geq\sum_{k\in\mathcal{K}}\bar{R}_{{\rm c},k} \tag{35b}$$

$$\frac{1-\bar{\xi}_{{\rm p},k}}{\ln 2}\geq\bar{R}_{{\rm p},k} \tag{35c}$$

$$(34c),(19d),(19e),(9b),(7),$$

where $\bar{\mathbf{G}}=\left\{g_{{\rm c},k}^{l},g_{{\rm p},k}^{l}|k\in\mathcal{K},1\leq l\leq L\right\}$ and $\bar{\mathbf{U}}=\left\{u_{{\rm c},k}^{l},u_{{\rm p},k}^{l}|k\in\mathcal{K},1\leq l\leq L\right\}$ are the scaling equalizer sets. The optimal $g_{{\rm c},k}^{l},g_{{\rm p},k}^{l}$ can be obtained from (13) based on a specific $\mathbf{h}_k^l$. The optimal $u_{{\rm c},k}^{l},u_{{\rm p},k}^{l}$ can be obtained from (17) based on $\mathbf{h}_k^l$.

The block-wise convex property still holds. As a result, we have the SAA-BCD algorithm as follows.

1) *The optimization of* $(\bar{\mathbf{G}},\bar{\mathbf{U}})$.
2) *The optimization of* $\mathbf{w}$*:* The optimal $\mathbf{w}$ can be obtained by solving the following problem.

$$\max_{\mathbf{w},s,\bar{\mathbf{R}}_{\rm c},\bar{\mathbf{R}}_{\rm p}} \quad s \tag{36}$$
$$\text{s.t.} \quad (35b),\ (35c),\ (19d),\ (9b),(7),$$

where $\bar{\xi}_{{\rm c},k}$ and $\bar{\xi}_{{\rm p},k}$ are given in (38).

3) *The optimization of* $\mathbf{v}$*:* The optimal $\mathbf{v}$ can be obtained by solving the following problem.

$$\max_{\mathbf{v},s,\bar{\mathbf{R}}_{\rm c},\bar{\mathbf{R}}_{\rm u}} \quad s \tag{37}$$
$$\text{s.t.} \quad (35b),\ (35c),\ (19d),\ (7),$$
$$|v_i|^2\leq 1,\forall i.$$

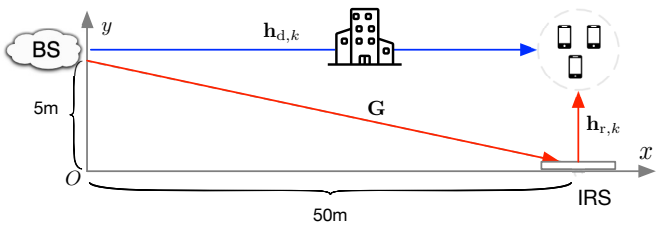

Fig. 2: Illustration of the RIS-assisted network architecture.

where $\bar{\xi}_{{\rm c},k}$ and $\bar{\xi}_{{\rm p},k}$ are given in (39).

The penalty-based BCD algorithm for the imperfect CSI case can be similarly derived. We leave this out due to limit of space.

V. Simulation Study

We consider a RIS-assisted communication scenario as depicted in Fig. 2. The parameters and channels are set the same as [31]. In this x-y plane, the RIS is located at location $(50,0)$m. The UEs are located randomly in a circle around center $(50,5)$m with a radius of 3m. The BS is located at the origin $(0,5)$m. The channel coefficients are a combination of distance-dependent large-scale fading and small-scale fading. The large-scale path loss model follows ${\rm PL}(d)=Ad^{-\alpha}$, where $A=-30$dB is the path loss at a reference distance 1m, d is the distance between the transmitter and receiver, and α is the path loss component. The path loss components for channels $\mathbf{h}_{{\rm r},k}$, $\mathbf{h}_{{\rm d},k}$, and $\mathbf{G}$ are set to 2.2, 3.5, and 2.2, respectively. For small-scale fading, the Rayleigh fading is assumed for the direct channel $\mathbf{h}_{{\rm d},k}$ and the Rician fading is assumed for the RIS reflected channels, i.e.,

$$\mathbf{h}_{{\rm d},k}=\sqrt{{\rm PL}(d)}\mathbf{h}_{{\rm d},k}^{\rm NLOS}$$

$$\mathbf{G}=\sqrt{\frac{{\rm PL}(d)}{K_G+1}}\left(\sqrt{K_G}\mathbf{G}^{\rm LOS}+\mathbf{G}^{\rm NLOS}\right)$$

$$\mathbf{h}_{{\rm r},k}=\sqrt{\frac{{\rm PL}(d)}{K_R+1}}\left(\sqrt{K_R}\mathbf{h}_{{\rm r},k}^{\rm LOS}+\mathbf{h}_{{\rm r},k}^{\rm NLOS}\right)$$

where $K_G=K_R=3$ is the Rician factors, $\mathbf{G}^{\rm LOS}$ and $\mathbf{h}_{{\rm r},k}^{\rm LOS}$ are line-of-sight (LoS) components, $\mathbf{h}_{{\rm d},k}^{\rm NLOS}$, $\mathbf{G}^{\rm NLOS}$ and $\mathbf{h}_{{\rm r},k}^{\rm NLOS}$ are the non line-of-sight (NLOS) components.

The noise power σ^2 is set to -90dBm. The SNR metric is defined as P/σ_0^2. For the proposed BCD algorithm and Algorithm 1, the stopping criteria is $\epsilon=0.01$. For Algorithm 1, the value of dual variables is $\rho=200$ and the scaling constant is $c=0.1$. Every simulated curve is obtained by averaging over 100 channel realizations.

We compare the performance of the following algorithms.

1) **RS:$\mathbf{\Phi_1}$**. RIS-assisted RS where the reflecting elements can be adjusted with continuous phase and amplitude.
2) **RS:$\mathbf{\Phi_2}$**. RIS-assisted RS where the reflecting elements can be adjusted with continuous phase only.
3) **RS:random phase**. RIS-assisted RS where the reflecting elements on the RIS are randomly set.
4) **RS:w/o phase**. RS only without RIS and there is only a direct channel between the UE and BS.

$$\bar{\xi}_{\mathrm{c},k}(\mathbf{w}) = \frac{1}{L}\sum_{l=1}^{L} u_{\mathrm{c},k}^{l}\left[|g_{\mathrm{c},k}^{l}|^2\left(\sum_{i\in\mathcal{M}}\mathbf{w}_i^H\mathbf{h}_k^l\mathbf{h}_k^{l,H}\mathbf{w}_i+\sigma_0^2\right)-2\mathrm{Re}(g_{\mathrm{c},k}^{l}\mathbf{h}_k^{l,H}\mathbf{w}_{\mathrm{c}})+1\right]-\frac{1}{L}\sum_{l=1}^{L}\ln(u_{\mathrm{c},k}^{l}), \tag{38a}$$

$$\bar{\xi}_{\mathrm{p},k}(\mathbf{w}) = \frac{1}{L}\sum_{l=1}^{L} u_{\mathrm{p},k}^{l}\left[|g_{\mathrm{p},k}^{l}|^2\left(\sum_{i\in\mathcal{K}}\mathbf{w}_i^H\mathbf{h}_k^l\mathbf{h}_k^{l,H}\mathbf{w}_i+\sigma_0^2\right)-2\mathrm{Re}(g_{\mathrm{p},k}^{l}\mathbf{h}_k^{l,H}\mathbf{w}_{k})+1\right]-\frac{1}{L}\sum_{l=1}^{L}\ln(u_{\mathrm{p},k}^{l}). \tag{38b}$$

$$\begin{aligned}\bar{\xi}_{\mathrm{c},k}(\mathbf{v}) = &\frac{1}{L}\sum_{l=1}^{L} u_{\mathrm{c},k}^{l}\left[|g_{\mathrm{c},k}^{l}|^2\left(\mathbf{v}^H\mathbf{Q}_{\mathrm{c},k}^{l}\mathbf{v}+2\mathrm{Re}\left(\mathbf{v}^H\mathbf{q}_{\mathrm{c},k}^{l}\right)+\alpha_{\mathrm{c},k}^{l}+\sigma_0^2\right)-2\mathrm{Re}(g_{\mathrm{c},k}^{l}\mathbf{h}_{\mathrm{d},k}^{l,H}\mathbf{w}_{\mathrm{c}}+g_{\mathrm{c},k}^{l}\mathbf{v}^H\mathbf{H}_k^{l}\mathbf{w}_{\mathrm{c}})+1\right]\\&-\frac{1}{L}\sum_{l=1}^{L}\ln(u_{\mathrm{c},k}^{l}),\end{aligned} \tag{39a}$$

$$\begin{aligned}\bar{\xi}_{\mathrm{p},k}(\mathbf{v}) = &\frac{1}{L}\sum_{l=1}^{L} u_{\mathrm{p},k}^{l}\left[|g_{\mathrm{p},k}^{l}|^2\left(\mathbf{v}^H\mathbf{Q}_{\mathrm{p},k}^{l}\mathbf{v}+2\mathrm{Re}\left(\mathbf{v}^H\mathbf{q}_{\mathrm{p},k}^{l}\right)+\alpha_{\mathrm{p},k}^{l}+\sigma_0^2\right)-2\mathrm{Re}(g_{\mathrm{p},k}^{l}\mathbf{h}_{\mathrm{d},k}^{l,H}\mathbf{w}_{k}+g_{\mathrm{p},k}^{l}\mathbf{v}^H\mathbf{H}_k^{l}\mathbf{w}_{k})+1\right]\\&-\frac{1}{L}\sum_{l=1}^{L}\ln(u_{\mathrm{p},k}^{l}).\end{aligned} \tag{39b}$$

5) **SDMA:$\mathbf{\Phi_1}$**. RIS-assisted SDMA where the reflecting elements can be adjusted with continuous phase and amplitude.

Note that SDMA is a special case of the proposed RS system, where the common rate for all UEs is set to zero. The proposed BCD algorithm and penalty-based BCD can be easily adapted for the SDMA case.

A. Perfect CSI Case

1) Convergence of the Proposed Algorithm: In Fig. 3, we present the convergence performance of the BCD algorithm and the penalty-based BCD algorithm for $M = 2$, $K = 4$, $N = 20$, and $P = 20$dBm. For the BCD algorithm, the objective value is the max-min rate defined in (19). As can be seen, the max-min rates are monotonically increasing and converge very quickly (i.e., 4-5 iterations for SDMA:Φ_1 and 10-15 iterations for RS:Φ_1). For the penalty-based BCD algorithm, the objective function value is the max-min rate minus the penalty term (see (26a)). Both the outer loop iteration and the inner loop iteration of the algorithm are counted. Due to the penalty factor, the objective function value fluctuates over iterations. This is because the inner loop is indeed the BCD algorithm, hence the objective value function keeps increasing in each inner loop. The convergence of the inner loop is guaranteed. However, the outer loop refines the penalty term, which may cause a decrease in the objective function value. Such refinement brings fluctuations over iterations. Eventually, the penalty term will go to zero to ensure that $\mathbf{u} = \mathbf{v}$ and the penalty-based BCD algorithm will converge after finite steps.

2) Impact of the Number of RIS Reflecting Elements: To compare the performance of different algorithms, we plot the max-min rate versus the number of reflecting elements on the RIS in Fig. 4. It can be seen that the performance of RS:Φ_1 is very close to that of RS:Φ_2, which means in practice we do not need an accurate RIS amplitude controller. Instead, a RIS where the phase shift can be adjusted works pretty well. Second, with the increase of the number of N, the performance of RS:Φ_1 and RS:Φ_2 increases, which suggests that by properly configuring more reflecting elements on the RIS, an improved max min rate performance can be achieved in RIS-assisted RS. As a comparison, the performance of RS: w/o phase and RS: random phase stays on a horizontal line. This shows that the introduction of RIS would not bring significant performance gains to the RS system if the reflecting elements on the RIS are not properly configured. Finally, we take a look at the curve of RS:Φ_1 and SDMA:Φ_1, their performance gap increases from 1.3 bits/s/Hz to 1.8 bits/s/Hz when N increases from 10 to 50. This experiment suggests that the RIS-assisted RS system exhibits significant performance gains over the RIS-assisted SDMA system.

3) Impact of the Transmit Power: Fig. 5 presents the max-min rate performance versus the transmit power for a system with $M = 2$, $K = 4$, and $N = 20$. It is shown that the performance of RS:Φ_1 and RS:Φ_2 increases with P almost linearly. For example, when P increased from 0dBm to 20dBm, the max-min rate increased from 0.55 bits/s/Hz to 2.5 bits/s/Hz. As a comparison, the max-min rate for SDMA: Φ_1 only slightly increased from 0.5 bits/s/Hz to 1 bits/s/Hz. This experiment shows that increasing the transmit power is more appealing to RS than SDMA in terms of performance improvement. Besides, we note that the performance of RS: random phase and RS: w/o phase is inferior to that of RS:Φ_1 and the performance gap is around 0.45 bits/s/Hz.

4) Impact of the Number of BS Antennas: The impact of the number of BS antennas on the max-min rate is shown in Fig. 6. The system parameters are set as $K = 4$, $N = 20$ and $P = 20$dBm. As can be seen, the max-min rate for all the schemes increases with M. This is because with more antennas at the BS deployed, an increased MIMO multiplexing gain can be expected. Moreover, we note that there is a turning point at $M = 4$ for SDMA: Φ_1 and RS: Φ_1 (RS: Φ_2). When

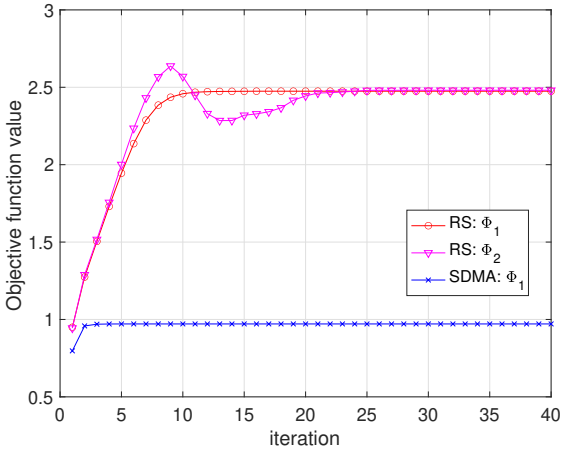

Fig. 3: The objective function value versus the number of iterations for $M = 2$, $K = 4$, $N = 20$, and $P = 20$dBm.

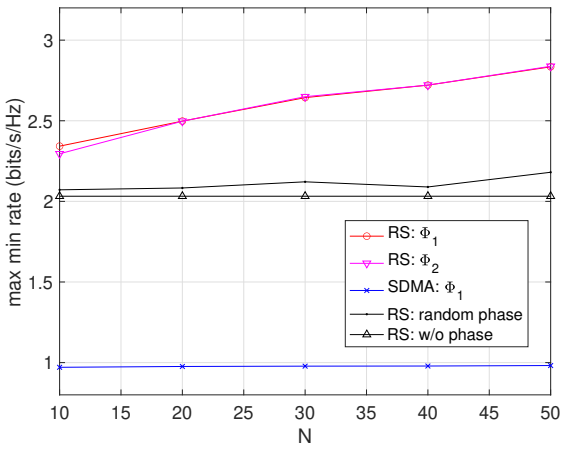

Fig. 4: Max-min rate versus the number of RIS elements N for $M = 2$, $K = 4$, and $P = 20$dBm.

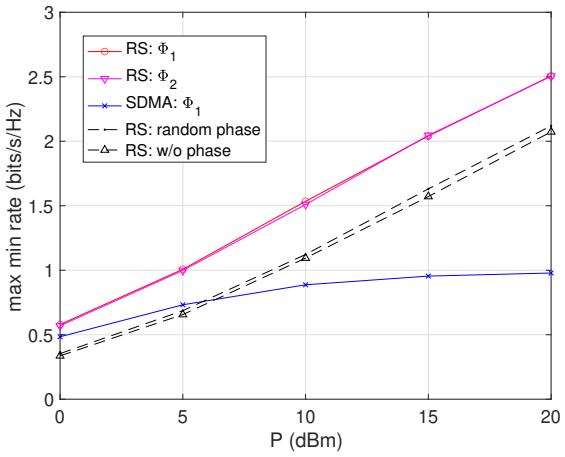

Fig. 5: Max-min rate versus the transmit power P at the BS for $M = 2$, $K = 4$, and $N = 20$.

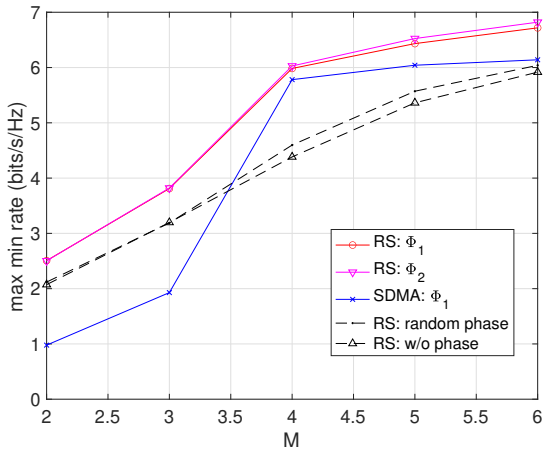

Fig. 6: Max-min rate versus the number of antennas M at the BS for $K = 4$, $N = 20$, and $P = 20$dBm.

$M < K$, the performance gap between SDMA: Φ_1 and RS: Φ_1 is around 1.6 bits/s/Hz. When $M \geq K$, the performance gap between SDMA: Φ_1 and RS: Φ_1 decreased significantly. The results suggest that RIS-assisted RS is more attractive than RIS-assisted SDMA in over-loaded systems where the number of antennas at the BS is less than the number of single-antenna users ($M < K$). In a MIMO system where $M = K$, RIS-assisted RS does not bring significant performance gains compared with the conventional RIS-assisted SDMA in terms of the max-min fairness. We will discuss this in detail in Section V-B.

5) Impact of the Number of UEs: Fig. 7 illustrates the impact of the number of UEs on the max-min rate performance when $M = 2$, $N = 20$, and $P = 20$dBm. The max-min rate decreases with the increase of the number of UEs due to inter-UE interference. In this experiment, we set $M = 2$. As can be seen, the performance of SDMA: Φ_1 is close to that of RS: Φ_1 when $M = K$. This is because in an under-loaded system ($M \geq K$) where the number of antennas at the BS is larger than or equal to the number of single-antenna users, zero-forcing (ZF) beamforming can be used to fully eliminate the interference in the $M \times K$ MIMO channel for both SDMA and RS system [19], [37].

6) Comparison with NOMA: We compare the performance of the proposed scheme with the RIS-assisted NOMA system in Fig. 8. The parameters are set as $M = 2$, $K = 3$, and $P = 20$dBm. The joint beamforming design for the RIS-assisted NOMA system is implemented with the semidefinite relaxation (SDR) method in [31] by changing the objective function to the max-min rate. Compared with RS transmission, NOMA requires ordering the channels based on channel gains so that the UE with a stronger channel gain can decode the UE's signal with a weaker channel gain. However, when combined with RIS configuration, the channels can be modified by the RIS. As a result, RIS-assisted NOMA needs to consider $K!$ different decoding orders, solve the beamforming separately for each decoding order, and select the best beamforming scheme. The complexity would be quite high especially when the number of UEs is large. Although some user ordering schemes are designed to reduce the complexity, they inevitably suffer certain performance loss [38]. Unlike NOMA, RS does not require channel ordering, and hence the complexity can be

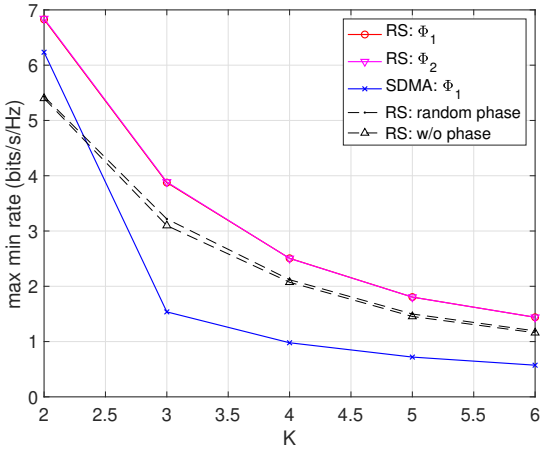

Fig. 7: Max-min rate versus the number of users K for $M = 2$, $N = 20$, and $P = 20$dBm.

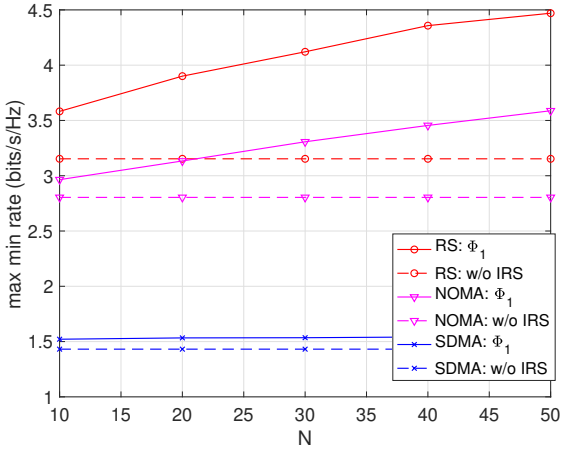

Fig. 8: Max-min rate versus the number of reflecting elements N for $M = 2$, $K = 3$, and $P = 20$dBm.

greatly reduced. With the increase of the number of reflecting elements on the RIS, the max-min rates of SDMA, NOMA, and RS all increase. Compared with SDMA and NOMA, the RS rate increases at a higher speed and achieves the best performance. To be specific, when the number of reflecting elements on the RIS increases from 10 to 50, the max-min rate improvement for RS, NOMA, and SDMA is given by about 0.9, 0.6 and 0.1 bits/s/Hz. This experiment suggests the advantages of RIS-assisted RS over RIS-assisted NOMA in terms of both performance and complexity.

B. Imperfect CSI case

For each channel generation $\mathbf{h}_k$, we can have a channel estimation as $\hat{\mathbf{h}}_k = \mathbf{h}_k - \Delta\mathbf{h}_k$. Based on the conditional probability $f_{\mathbf{h}_k|\hat{\mathbf{h}}_k}(\mathbf{h}_k|\hat{\mathbf{h}}_k)$, we set $L = 100$ channel realizations realizations. Note that $\mathbf{h}_k$ represents the actual channel experienced by user k but is unknown to the BS while $\hat{\mathbf{h}}_k^l (1 \leq l \leq L)$ can be used to calculate the sample average rate, which can approximate the ergodic max min rate performance.

1) Impact of the transmit power: We compare the ergodic max-min performance of RS:ϕ_1 with that of SDMA:ϕ_1 by changing the transmit power. In Fig. 9, Fig. 10, and Fig. 11, we show their performance by fixing the number of transmit antennas on the RIS to be 20 and changing the relative channel estimation errors.

Fig. 9 shows the performance of an overloaded system where $M = 2, K = 4$ and $M < K$. It can be seen that with the increase of the transmit power, the performance of RIS-assisted SDMA slowly increases while the performance of RIS-assisted RS increases significantly, regardless of the value of the relative channel uncertainties. The proposed scheme is quite robust toward channel uncertainties. For example, when the transmit power is 20dBm and the relative CSI error is 0.1, the max-min rate of RS is around 2.2 bits/s/Hz, which is 88% of the rate achieved at perfect CSI case (2.5 bits/s/Hz). Even when the relative CSI error is quite large ($\delta = 0.5$, the proposed RS scheme still achieves 1.75 bits/s/Hz, which is around 70% of the perfect CSI case.)

Fig. 10 presents the performance of a system where $M = K = 3$. In the perfect CSI case, we observe that the curve for RS and SDMA almost overlapped. This can be explained by the max-min-fairness (MMF) degree-of-freedom (DOF) analysis in [9], [19], [39] from an information theoretic perspective. The MMF-DOF represents the maximum multiplexing gain that can be simultaneously achieved by all the UEs. When $M \geq K$, ZF can be used to fully eliminate the interference in the combined $M \times K$ MIMO channel for both SDMA and RS. Hence RIS-assisted RS and RIS-assisted SDMA achieves similar performance under the setting of $M = K = 3$. However, when the relative CSI error gets larger, the performance of SDMA decreases significantly, and the RS scheme is much more robust. To be specific, when the transmit power is 20dBm, the max-min rate for RS (perfect CSI) and SDMA (perfect CSI) is around 6.4 bits/s/Hz and 6.0 bits/s/Hz, respectively. When the CSI error is large, i.e., $\delta = 0.5$, RS still achieves 2.84 bits/s/Hz, which is 44% the performance in the perfect CSI case. SDMA only achieves 1.57 bits/s/Hz, which is only 26% the performance of the perfect CSI case. This experiment suggests that RS is more robust to the CSI uncertainties compared with SDMA, even when $M \geq K$.

Fig. 11 shows the performance of an under-loaded system where $M > K$. It can be seen that SDMA and RS show very similar performance in the low SNR regime under perfect CSI. However, as the relative CSI error grows, the performance of SDMA decreases significantly. When the transmit power is 20dBm, the max-min rate for RS is around 5.0 bits/s/Hz (or 75% of the performance in the perfect CSI case) while the max min rate for SDMA is only 3.27 bits/s/Hz (or 50% of the performance on the perfect CSI case). The experiment again shows that RS has the advantage of being robust with imperfect CSI. Meanwhile, as RIS only consists of passive elements, accurately obtaining the CSI is quite challenging. Therefore, it is a perfect fit for RS to integrate with RIS technology.

2) Impact of the number of RIS reflecting elements: We plot the max-min performance versus the number of reflecting

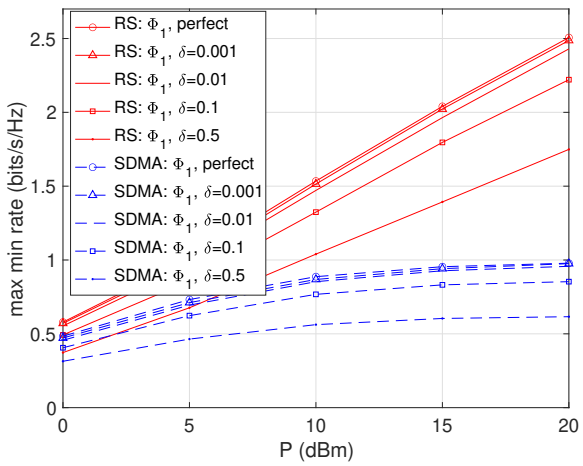

Fig. 9: Max-min rate versus transmit power for $M = 2$, $K = 4$, and $N = 20$ under imperfect CSI case.

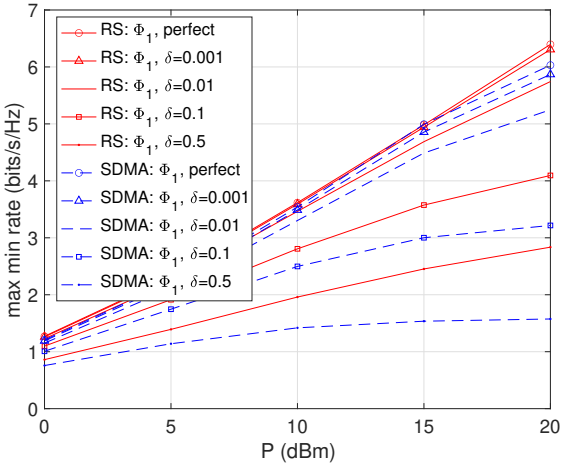

Fig. 10: Max-min rate versus transmit power for $M = 3$, $K = 3$, and $N = 20$ under imperfect CSI case.

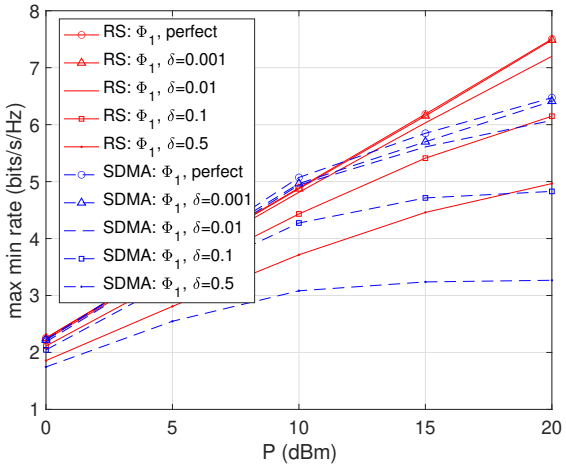

Fig. 11: Max-min rate versus transmit power for $M = 4$, $K = 2$, and $N = 20$ under imperfect CSI case.

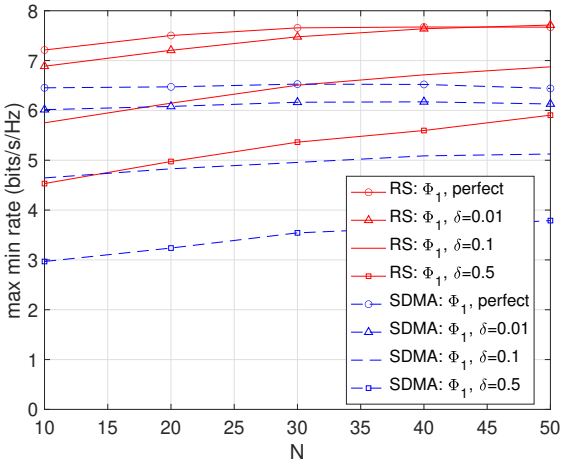

Fig. 12: Max-min rate versus transmit power for $M = 4$, $K = 2$, and $P = 20$dbm under imperfect CSI case.

elements on the RIS in Fig. 12. When the relative CSI error is large, i.e., $\delta = 0.5$, the performance of both SDMA and RS improves with the increase of N. To be specific, for RS, the performance gap from the perfect CSI case decreased from $7.2 - 4.5 = 2.7$ bits/s/Hz when $N = 10$ to $7.7 - 5.9 = 1.8$ bits/s/Hz when $N = 50$. For SDMA, the performance gap from the perfect CSI case decreased from $6.5 - 3 = 3.5$ bits/s/Hz when $N = 10$ to $6.4 - 3.8 = 2.6$ bits/s/Hz when $N = 50$. When the relative CSI error is small, i.e., $\delta = 0.01$, with the increase of N, for RS the performance gap from the perfect CSI case almost vanished. However, for SDMA, the performance gap always exists. This experiment suggests that when the CSI uncertainty is small, it is possible that RS can achieve the same performance as the perfect CSI case when the number of reflecting elements on the RIS is large.

3) The impact of RIS configuration: In this experiment, we investigate the impact of RIS configuration. We compared the performance of RS:ϕ_1 with two benchmark algorithms, RS: random phase and RS: w/o phase. When the transmit power is high, i.e. $P = 20$dBm, as shown in Fig. 13, the max-min rate decreases with the increase of the relative CSI error. Increasing the number of reflecting elements on the RIS can improve the performance of RS:ϕ_1. However, the performance of RS with random phase does not improve significantly when N increases. In the perfect CSI case, i.e., $\delta = 0$, RS:ϕ_1 (N=50) achieves considerable performance gain (7.2-4.7=2.5 bits/s/Hz) compared with RS: w/o RIS. Even when the CSI error is $\delta = 0.01$, the performance gain is still 6.6-4.1=2.5 bits/s/Hz. When CSI error is large, i.e., $\delta = 0.5$, the performance gain becomes 3.6-2.3=1.3 bits/s/Hz. This shows that RS with properly configured RIS is quite robust toward a relatively small CSI error.

When the transmit power is low, i.e., $P = 0$dBM, the max-min rate performance of RS with different RIS configurations is shown in Fig. 14. It can be seen that RS: random phase achieves a small amount of performance gain compared with RS: w/o RIS, no matter whether the relative CSI error is small or large. RS:ϕ_1 achieves a max-min rate at around 2 bits/s/Hz when $N = 50$ and $\delta = 0.01$, which is almost three times the max-min rate achieved by RS without RIS. This

further demonstrates the benefits of integrating RIS and RS. Moreover, comparing Fig. 13 and Fig. 14, we notice that the benefit of increasing the reflecting elements on the RIS is more significant at a low SNR regime or when the transmit power is small. To be specific, when $P = 0$dBm and $\delta = 0.01$, the performance gain of increasing N from 20 to 50 is (2.0-1.2)/1.2=66.7% for RS:ϕ_1 while this number is (6.6-5.7)/5.7 =15.8% when $P = 20$dBm and $\delta = 0.01$.

VI. Conclusions

This paper has investigated the interplay between RS and RIS. A BCD algorithm is developed to maximize the minimum rate of all users. Compared with the conventional SDR-based method, the proposed method does not suffer from the rank-one problem. Our simulation results show that with the proposed method, RIS-assisted RS could achieve a satisfactory performance compared with conventional multiple access technologies, such as SDMA and NOMA with/without RIS. An SAA-BCD algorithm is also developed to perform joint beamforming design in the imperfect CSI case. Our simulation results suggest that RS has the advantage of being robust with channel uncertainties and is a good fit to RIS-assisted networks.

References

[1] Q. Wu and R. Zhang, "Towards smart and reconfigurable environment: Intelligent reflecting surface aided wireless network," *IEEE Commun. Mag.*, vol. 58, no. 1, pp. 106–112, Jan. 2019.

[2] M. Di Renzo *et al.*, "Smart radio environments empowered by reconfigurable AI meta-surfaces: An idea whose time has come," *EURASIP J. Wireless Commun. Netw.*, vol. 2019, no. 1, Article no.: 129, May 2019.

[3] C. Huang, A. Zappone, G. C. Alexandropoulos, M. Debbah, and C. Yuen, "Reconfigurable intelligent surfaces for energy efficiency in wireless communication," *IEEE Trans. Wireless Commun.*, vol. 18, no. 8, pp. 4157–4170, Aug. 2019.

[4] Y. Xu, G. Yue, and S. Mao, "User grouping for massive MIMO in FDD systems: New design methods and analysis," *IEEE Access J.*, vol. 2, no. 1, pp. 947–959, Sept. 2014.

[5] M. Dai, B. Clerckx, D. Gesbert, and G. Caire, "A rate splitting strategy for massive MIMO with imperfect CSIT," *IEEE Trans. Wireless Commun.*, vol. 15, no. 7, pp. 4611–4624, July 2016.

[6] B. Clerckx, H. Joudeh, C. Hao, M. Dai, and B. Rassouli, "Rate splitting for MIMO wireless networks: A promising PHY-layer strategy for LTE evolution," *IEEE Commun. Mag.*, vol. 54, no. 5, pp. 98–105, May 2016.

[7] H. Joudeh and B. Clerckx, "Robust transmission in downlink multiuser MISO systems: A rate-splitting approach," *IEEE Trans. Signal Process.*, vol. 64, no. 23, pp. 6227–6242, Dec. 2016.

[8] Y. Mao, O. Dizdar, B. Clerckx, R. Schober, P. Popovski, and H. V. Poor, "Rate-splitting multiple access: Fundamentals, survey, and future research trends," *arXiv preprint arXiv:2201.03192*, Apr. 2022. [Online]. Available: https://arxiv.org/abs/2201.01471

[9] Y. Mao, B. Clerckx, and V. O. Li, "Rate-splitting multiple access for downlink communication systems: Bridging, generalizing, and outperforming SDMA and NOMA," *EURASIP J. Wireless Commun. Netw.*, vol. 2018, no. 1, Article no.: 133, May 2018.

[10] H. Joudeh and B. Clerckx, "Sum-rate maximization for linearly precoded downlink multiuser MISO systems with partial CSIT: A rate-splitting approach," *IEEE Trans. Commun.*, vol. 64, no. 11, pp. 4847–4861, Nov. 2016.

[11] H. Fu, S. Feng, W. Tang, and D. W. K. Ng, "Robust secure beamforming design for two-user downlink MISO rate-splitting systems," *IEEE Trans. Wireless Commun.*, vol. 19, no. 12, pp. 8351–8365, Dec. 2020.

[12] K. Weinberger, A. A. Ahmad, A. Sezgin, and A. Zappone, "Synergistic benefits in IRS-and RS-enabled C-RAN with energy-efficient clustering," *IEEE Trans. Wireless Commun.*, vol. 21, no. 10, pp. 8459–8475, Oct. 2022.

[13] Z. Yang, J. Shi, Z. Li, M. Chen, W. Xu, and M. Shikh-Bahaei, "Energy efficient rate splitting multiple access (RSMA) with reconfigurable intelligent surface," in *Proc. IEEE ICC 2020 Workshops*, Virtual Conference, June 2020, pp. 1–6.

[14] Y. Gao, Q. Wu, W. Chen, and D. W. K. Ng, "Rate-splitting multiple access for intelligent reflecting surface-aided secure transmission," *arXiv preprint arXiv:2208.09818*, Nov. 2022. [Online]. Available: https://arxiv.org/abs/2208.09818

[15] T. Fang, Y. Mao, S. Shen, Z. Zhu, and B. Clerckx, "Fully connected reconfigurable intelligent surface aided rate-splitting multiple access for multi-user multi-antenna transmission," *arXiv preprint arXiv:2201.07048*, Mar. 2022. [Online]. Available: https://arxiv.org/abs/2201.07048

[16] A. Bansal, K. Singh, B. Clerckx, C.-P. Li, and M.-S. Alouini, "Rate-splitting multiple access for intelligent reflecting surface aided multi-user communications," *IEEE Trans. Veh. Technol.*, vol. 70, no. 9, pp. 9217–9229, Sept. 2021.

[17] H. Li, Y. Mao, O. Dizdar, and B. Clerckx, "Rate-splitting multiple access for 6G–part III: Interplay with reconfigurable intelligent surfaces," *arXiv preprint arXiv:2205.02036*, Aug. 2022. [Online]. Available: https://arxiv.org/abs/2205.02036

[18] Z. Wang, L. Liu, and S. Cui, "Channel estimation for intelligent reflecting surface assisted multiuser communications: Framework, algorithms, and analysis," *IEEE Trans. Wireless Commun.*, vol. 19, no. 10, pp. 6607–6620, Oct. 2020.

[19] B. Clerckx *et al.*, "Is NOMA efficient in multi-antenna networks? a critical look at next generation multiple access techniques," *arXiv preprint arXiv:2101.04802*, Jan. 2021. [Online]. Available: https://arxiv.org/abs/2101.04802

[20] A. S. de Sena, P. H. Nardelli, D. B. da Costa, P. Popovski, and C. B. Papadias, "Rate-splitting multiple access and its interplay with intelligent reflecting surfaces," *IEEE Commun. Mag.*, vol. 60, no. 7, pp. 52–57, July 2022.

[21] Q. Wu, S. Zhang, B. Zheng, C. You, and R. Zhang, "Intelligent reflecting surface-aided wireless communications: A tutorial," *IEEE Trans. Commun.*, vol. 69, no. 5, pp. 3313–3351, May 2021.

[22] Z. Ding, X. Lei, G. K. Karagiannidis, R. Schober, J. Yuan, and V. K. Bhargava, "A survey on non-orthogonal multiple access for 5G networks: Research challenges and future trends," *IEEE J. Sel. Areas Commun.*, vol. 35, no. 10, pp. 2181–2195, Oct. 2017.

[23] F. Fang, Y. Xu, Q.-V. Pham, and Z. Ding, "Energy-efficient design of IRS-NOMA networks," *IEEE Trans. Veh. Technol.*, vol. 69, no. 11, pp. 14 088–14 092, Nov. 2020.

[24] Y. Cheng, K. H. Li, Y. Liu, K. C. Teh, and H. V. Poor, "Downlink and uplink intelligent reflecting surface aided networks: NOMA and OMA," *IEEE Trans. Wireless Commun.*, vol. 20, no. 6, pp. 3988–4000, June 2021.

[25] Z. Ding and H. V. Poor, "A simple design of IRS-NOMA transmission," *IEEE Commun. Lett.*, vol. 24, no. 5, pp. 1119–1123, May 2020.

[26] Z. Li, C. Ye, Y. Cui, S. Yang, and S. Shamai, "Rate splitting for multi-antenna downlink: Precoder design and practical implementation," *IEEE J. Sel. Areas Commun.*, vol. 38, no. 8, pp. 1910–1924, Aug. 2020.

[27] H. Xia, Y. Mao, X. Zhou, B. Clerckx, S. Han, and C. Li, "Secure beamforming design for rate-splitting multiple access in multi-antenna broadcast channel with confidential messages," *arXiv preprint arXiv:2202.07328*, Feb. 2022. [Online]. Available: https://arxiv.org/abs/2202.07328

[28] D. Yu, S.-H. Park, O. Simeone, and S. Shamai, "Robust design of rate-splitting multiple access with imperfect CSI for cell-free MIMO systems," *arXiv preprint arXiv:2203.03690*, Mar. 2022. [Online]. Available: https://arxiv.org/abs/2203.03690

[29] B. Matthiesen, Y. Mao, P. Popovski, and B. Clerckx, "Globally optimal beamforming for rate splitting multiple access," in *Proc. IEEE ICASSP 2021*, Virtual Conference, June 2021, pp. 4775–4779.

[30] H. Fu, S. Feng, and D. W. K. Ng, "Resource allocation design for IRS-aided downlink MU-MISO RSMA systems," in *Proc. IEEE ICC 2021 Workshops*, Virtual Conference, June 2021, pp. 1–6.

[31] X. Mu, Y. Liu, L. Guo, J. Lin, and N. Al-Dhahir, "Exploiting intelligent reflecting surfaces in NOMA networks: Joint beamforming optimization," *IEEE Trans. Wireless Commun.*, vol. 19, no. 10, pp. 6884–6898, Oct. 2020.

[32] Z. Lin, M. Lin, T. de Cola, J.-B. Wang, W.-P. Zhu, and J. Cheng, "Supporting IoT with rate-splitting multiple access in satellite and aerial integrated networks," *IEEE Internet of Things J.*, vol. 8, no. 14, pp. 11 123–11 134, July 2021.

[33] Y. Nesterov and A. Nemirovskii, *Interior-point Polynomial Algorithms in Convex Programming*. Philadelphia, PA: SIAM, 1994.

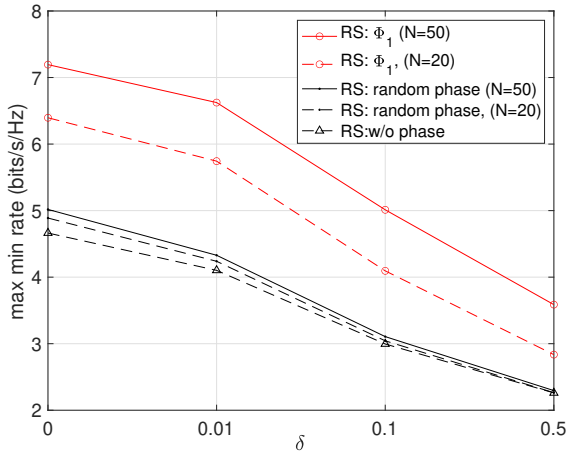

Fig. 13: Max-min rate versus relative CSI error for $M = 3$, $K = 3$, and $P = 20$dbm.

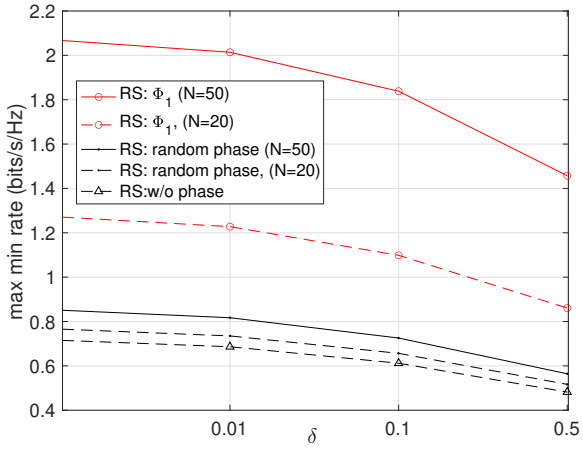

Fig. 14: Max-min rate versus relative CSI error for $M = 3$, $K = 3$, and $P = 0$dbm.

[34] Y. Omid, S. M. Shahabi, C. Pan, Y. Deng, and A. Nallanathan, "Low-complexity robust beamforming design for IRS-aided MISO systems with imperfect channels," *IEEE Commun. Lett.*, vol. 25, no. 5, pp. 1697–1701, May 2021.

[35] G. Zhou, C. Pan, H. Ren, K. Wang, and A. Nallanathan, "A framework of robust transmission design for IRS-aided MISO communications with imperfect cascaded channels," *IEEE Trans. Signal Process.*, vol. 68, pp. 5092–5106, Aug. 2020.

[36] S. Hong, C. Pan, H. Ren, K. Wang, K. K. Chai, and A. Nallanathan, "Robust transmission design for intelligent reflecting surface-aided secure communication systems with imperfect cascaded csi," *IEEE Trans. Wireless Commun.*, vol. 20, no. 4, pp. 2487–2501, Aug. 2020.

[37] N. Jindal and A. Goldsmith, "Dirty-paper coding versus TDMA for MIMO broadcast channels," *IEEE Trans. Inf. Theory*, vol. 51, no. 5, pp. 1783–1794, May 2005.

[38] Y. Yang, B. Zheng, S. Zhang, and R. Zhang, "Intelligent reflecting surface meets OFDM: Protocol design and rate maximization," *IEEE Trans. Commun.*, vol. 68, no. 7, pp. 4522–4535, July 2020.

[39] H. Joudeh and B. Clerckx, "Rate-splitting for max-min fair multigroup multicast beamforming in overloaded systems," *IEEE Trans. Wireless Commun.*, vol. 16, no. 11, pp. 7276–7289, Nov. 2017.

Ticao Zhang received the B.E. degree in 2014 and the M.S. degree in 2017 from the School of Electronic Information and Communications, Huazhong University of Science and Technology, Wuhan, China. He received a Ph.D. degree in Electrical and Computer Engineering at Auburn university, Auburn, AL, USA in 2022. Currently, he is a Research Scientist with Ericsson Inc., Santa Clara, CA. His research interest includes video coding and communications, machine learning, and optimization and design of next generation wireless networks. His paper was featured as IEEE Access Journal's "Article of the Week" in Apr. 2020.

Shiwen Mao [S'99-M'04-SM'09-F'19] received his Ph.D. in electrical engineering from Polytechnic University, Brooklyn, NY in 2004. Currently, he is a Professor and Earle C. Williams Eminent Scholar in Electrical and Computer Engineering at Auburn University, Auburn, AL, USA. His research interest includes wireless networks, multimedia communications, and smart grid. He is a Distinguished Lecturer of IEEE Communications Society (2021-2022) and IEEE Council of RFID (2021-2022), and was a Distinguished Lecturer (2014-2018) and a Distinguished Speaker (2018-2021) of IEEE Vehicular Technology Society. He received the 2023 SEC Faculty Achievement Award for Auburn, the IEEE ComSoc TC-CSR Distinguished Technical Achievement Award in 2019, the Auburn University Creative Research & Scholarship Award in 2018, the NSF CAREER Award in 2010, and several service awards from IEEE ComSoc. He is a co-recipient of the 2022 Best Journal Paper Award of IEEE ComSoc eHealth Technical Committee (TC), the 2021 Best Paper Award of Elsevier/KeAi Digital Communications and Networks Journal, the 2021 IEEE Internet of Things Journal Best Paper Award, the 2021 IEEE Communications Society Outstanding Paper Award, the IEEE Vehicular Technology Society 2020 Jack Neubauer Memorial Award, the 2018 Best Journal Paper Award and the 2017 Best Conference Paper Award from IEEE ComSoc Multimedia TC, and the 2004 IEEE Communications Society Leonard G. Abraham Prize in the Field of Communications Systems. He is a co-recipient of the Best Paper Awards from IEEE ICC 2022 and 2013, IEEE GLOBECOM 2019, 2016, and 2015, and IEEE WCNC 2015, and the Best Demo Awards from IEEE INFOCOM 2022 and IEEE SECON 2017. He is the Editor-in-Chief of IEEE Transactions on Cognitive Communications and Networking and an Area Editor of ACM GetMobile. He was the General Chair of IEEE INFOCOM 2022, a TPC Chair of IEEE INFOCOM 2018, and a TPC Vice-Chair of IEEE GLOBECOM 2022.